Desalination and Water Treatment
www.deswater.com
doi: 10.1080/19443994.2013.773565

51 (2013) 7255–7268
November

Taylor & Francis
Taylor & Francis Group

Treatment of aqueous solution of antibiotics amoxicillin and cloxacillin by modified photo-Fenton process

Malay Chaudhuri, Muhammad Zulhasri Bin Abd Wahap, Augustine Chioma Affam*

Department of Civil Engineering, Universiti Teknologi PETRONAS, Bandar Seri Iskandar, 31750 Tronoh, Perak, Malaysia
Tel. +6010 384 970; +6019 518 6876; +60125 103 547; Fax: +605 365 6716; email: augustine_g01458@utp.edu.my

Received 10 September 2012; Accepted 1 February 2013

ABSTRACT

The study examined the effectiveness of the modified photo-Fenton (UV-vis/ferrioxalate/H_2O_2) process in treatment of an antibiotic aqueous solution. The optimum operating conditions for the treatment of a 300 mg/L antibiotic aqueous solution (150 mg/L of amoxicillin and 150 mg/L of cloxacillin) were obtained by using the central composite design of the response surface methodology. Under the optimum operating conditions (H_2O_2/chemical oxygen demand (COD) molar ratio 2.75, H_2O_2/Fe^{3+} molar ratio 75, $H_2O_2/C_2H_2O_4$ molar ratio 37.5, reaction time 90 min and pH 3), 78.37, 45.94, and 52.30% removal of COD, NH_3–N, and TOC, respectively, were achieved and the biodegradability (biochemical oxygen demand $(BOD)_5$/COD ratio) improved from 0 to 0.35. Model prediction and experimental removal efficiency were in agreement with < 5% error. The modified photo-Fenton process is effective in pretreatment of the antibiotic aqueous solution for biological treatment.

Keywords: Antibiotic; Amoxicillin; Cloxacillin; Modified photo-Fenton process; Response surface methodology

1. Introduction

Advanced oxidation processes (AOPs) constitute a promising technology for the treatment of water and wastewater containing non-easily removable organic compounds with high toxicity and low biodegradability [1]. Experiences with different oxidation technologies and substrates have shown that a partial oxidation of toxic water may increase its biodegradability up to high levels [2,3]. Oxidation with Fenton's reagent is based on hydroxyl radical ($OH^{\cdot}$) produced by catalytic decomposition of hydrogen peroxide (H_2O_2) in reaction with ferrous ion (Fe^{2+}) as in Eq. (1) [4].

$$H_2O_2 + Fe^{2+} \rightarrow Fe^{3+} + OH^- + OH^{\cdot} \quad (1)$$

In the UV photo-Fenton process, the rate of ($OH^{\cdot}$) formation is increased by photoreactions of H_2O_2 and/or Fe^{3+} that produce ($OH^{\cdot}$) directly or regenerate Fe^{2+} [5], thus increase the efficiency of the process. The modified photo-Fenton (UV–vis/ferrioxalate/H_2O_2) process has high degradation efficiency because the ferrioxalate is able to absorb light strongly at longer wavelength and generates ($OH^{\cdot}$) with high quantum yield [6]. The quantum yield of Fe^{2+} regeneration greatly increases when Fe^{2+} complexes with a carboxylic anion, such as oxalate [7]. The ferrioxalate complex, $Fe^{III}(C_2O_4)_3^{3-}$, is highly photosensitive and reduction of Fe^{3+} to Fe^{2+}, through a photoinduced

*Corresponding author.

ligand to metal charge transfer, can occur over the ultraviolet and into the visible (out to $\lambda \sim 550$ nm):

$$Fe^{III}(C_2O_4)_3^{3-} + h\nu \rightarrow Fe^{2+} + 2C_2O_4^{2-} + C_2O_4^{\cdot-} \quad (2)$$

$$C_2O_4^{\cdot-} \rightarrow CO_2^{\cdot-} + CO_2 \quad (3)$$

$$CO_2^{\cdot-} + Fe^{III}(C_2O_4)_3^{3-} \rightarrow Fe^{2+} + CO_2 + 3C_2O_4^{2-} \quad (4)$$

The reactions can be collapsed into one reaction, since the short lifetime of the oxyl radical, $C_2O_4^{\cdot-}$, should preclude it from participation in other reactions, and its decarboxylation product, $CO_2^{\cdot-}$, is not involved in any other significant reactions:

$$Fe^{III}(C_2O_4)_3^{3-} + h\nu \rightarrow Fe^{2+} + CO_2 + 2.5C_2O_4^{2-} \quad (5)$$

There are no other significant photochemical reactions (e.g. H_2O_2 photolysis) because the molar extinction coefficients of the reactants are such that ferrioxalate is the predominant absorber. The Fe^{2+} produced then generates ($OH^{\cdot}$) radical via the Fenton reaction:

$$Fe^2 + H_2O_2 + 3C_2O_4^{2-} \rightarrow Fe^{III}(C_2O_4)_3^{3-} + OH^- + OH^{\cdot} \quad (6)$$

In the presence of a sufficient excess of oxalate, Fe^{3+} will coordinate with either two or three oxalate ligands. As with the photo-Fenton reaction, iron cycles between oxidation states and so the production of hydroxyl radical is limited only by the availability of light, H_2O_2, and oxalate, the latter two of which are depleted during the reaction. UV-vis/ferrioxalate/H_2O_2 treatment of aniline wasterwater [8], dyehouse waste [9] and winery wastewater [10], and degradation of metal complex azo dyes [9], 2,4-D [11], diethylstilbestrol [12], reactive dyes [13,14], acid dye Orange II [15], and phenolic pollutants [16] have been reported. Amoxicillin and cloxacillin are semi-synthetic penicillin obtaining their antimicrobial properties from the presence of a beta-lactam ring. The presence of the antibiotics at low concentrations in the environment may develop antibiotic-resistant bacteria [17]. However, there is no report on modified photo-Fenton (UV-vis/ferrioxalate/H_2O_2) treatment of aqueous solution of the antibiotics amoxicillin and cloxacillin. This study examined UV-vis/ferrioxalate/H_2O_2 treatment of an aqueous solution of antibiotics amoxicillin and cloxacillin in terms of chemical oxygen demand (COD), ammonia-nitrogen (NH_3–N) and total organic carbon (TOC) removal and biodegradability (BOD_5/COD ratio) improvement. The treatment was optimized by using the central composite design (CCD) of the response surface methodology (RSM).

2. Materials and methods

2.1. Chemicals and antibiotics

Hydrogen peroxide (30%, w/w), oxalic acid ($C_2H_2O_4{\cdot}2H_2O$) and ferric sulfate ($Fe_2(SO_4)_3$) were purchased from R and M Marketing, Essex, U.K. The antibiotics amoxicillin and cloxacillin used to prepare aqueous solution were obtained from a commercial source and were used as received. Fig. 1 shows the chemical structure of amoxicillin and cloxacillin.

2.2. Analytical methods

COD was determined according to Method 5220D (closed reflux, colorimetric method) of the Standard Methods [18]. Where the sample contained hydrogen peroxide (H_2O_2), to reduce interference in COD determination pH was increased to above 10 so as to decompose hydrogen peroxide to oxygen and water [19,20]. TOC analyzer (Model 1,010, O & I Analytical) was used for determining TOC. The pH was measured by a pH

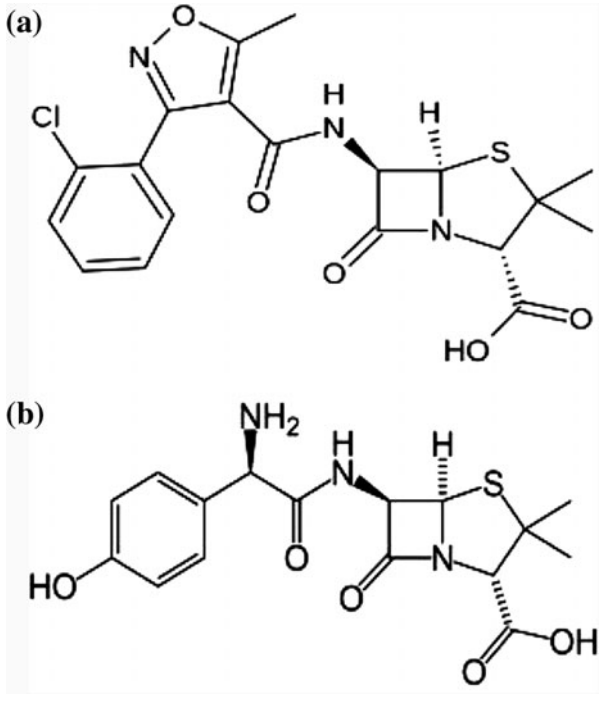

Fig. 1. Chemical structure of the antibiotics (a) amoxicillin (AMX) and (b) cloxacillin (CLX).

meter (HACH sension 4) and a pH electrode (HACH platinum series pH electrode model 51,910, HACH Company, USA). Biodegradability was measured by five day biochemical oxygen demand (BOD_5) test according to Method 5210B (seeding procedure) of the Standard Methods [18].The treated antibiotic aqueous solution was adjusted to pH 7 before the BOD_5 test. Ammonia-nitrogen (NH_3–N) was measured by the Nessler method [21]. DO was measured using YSI 5,000 dissolved oxygen meter. The seed for BOD_5 test was obtained from a municipal wastewater treatment plant.

2.3. Antibiotic aqueous solution

Antibiotic aqueous solution was 300 mg/L of antibiotics (150 mg/L of amoxicillin and 150 mg/L of cloxacillin) in distilled water. Concentration of penicillin formulation in real antibiotic wastewater has been reported to be up to 400 mg/L [22]. The antibiotic aqueous solution was prepared weekly and stored at 4°C. The antibiotic aqueous solution had COD of 392 mg/L, NH_3–N of 7.3 mg/L and TOC of 144.4 mg/L.

2.4. Experimental procedure

Batch experiments were conducted with 200 mL of the antibiotic aqueous solution in a 250 Pyrex beaker, placed in a SolSim solar simulator photoreactor (Luzchem Research Inc. Gloucester, ON, Canada) with solar intensity 0.85 kW/m^2. The required amount of $C_2H_2O_4$ and Fe^{3+} were added to the aqueous solution and mixed by a magnetic stirrer to ensure complete homogeneity during reaction. Thereafter, necessary amount of H_2O_2 was added to the mixture with simultaneous adjustment to pH 3 by using H_2SO_4 because maximum degradation of the antibiotics by Fenton and photo-Fenton processes was reported to be at pH 3 [23,24]. The time at which H_2O_2 was added to the mixture was considered as the beginning of the experiment. Samples were taken at preselected time intervals and filtered through 0.45-μm membrane filter for determination of COD, NH_3–N and TOC, and when required BOD_5.

2.5. Optimization and RSM

Design expert software Version 6.0.7 [25] was used for statistical design of experiment and data analysis. CCD of the RSM was used to optimize the operating conditions (variables) of the treatment because it is well suited for fitting a quadratic surface, which usually works well for process optimization and it is the experimental design mostly utilized for the development of analytical procedure as against three-level factorial design which is not frequently used and has been limited to the optimization of two variables [26]. The variables were simultaneously changed in a central composite circumscribed design. The values of the variables H_2O_2/COD molar ratio, H_2O_2/Fe^{3+} molar ratio, $H_2O_2/C_2H_2O_4$ molar ratio and reaction time were set at three levels: −1 (low), 0 (central) and +1 (high) and the total number of experiments with three factors was obtained as 30 ($2^k + 2k + 6$), where k is the number of factors (which equals 4 in this case). Twenty-four experiments were augmented with six replications at the design center to evaluate the pure error and carried in randomized order as required in the circumscribed composite design. The variables H_2O_2/COD molar ratio, H_2O_2/Fe^{2+} molar ratio, $H_2O_2/C_2H_2O_4$ molar ratio, and reaction time were studied in the range 1.5–4.0, 25–50, 50–100, and 60–120 min, respectively. Chosen response parameters for the process were removal of COD, NH_3–N, and TOC. Table 1 shows the experimental design and the responses. Regression models and statistical analysis, contour plots, normal probability plots, outlier T plots, and perturbation plots were made. Model terms were evaluated by the p-value (probability) with 95% confidence level. The quality of fit of the polynomial model was expressed by the coefficient of determination R^2. The optimum operating conditions (variables) were identified from the contour plots and response equation simultaneously. The following response equation describing an empirical second-order polynomial model was used to assess the predicted results:

$$Y = \beta_o + \sum_{i=1}^{k} \beta_i x_i + \sum_{i=1}^{k} \beta_{ii} x_i^2 + \sum_{i=1}^{k} \sum_{j=1}^{k} \beta_{ij} x_i x_j + \varepsilon \qquad (7)$$

where Y is the dependent response; β_o the constant coefficient; i, ii, and ij are the coefficients for the linear, quadratic, and interaction effect; x_i and x_j are the factors (i.e., H_2O_2/COD, H_2O_2/Fe^{3+} $H_2O_2/C_2H_2O_4$, molar ratio and reaction time); k signifies the number of independent variables and ε is the random error [26]. The result (Y) was calculated as the sum of a constant (β_o), four first-order effects (A, B, C, and D), four second-order effects (A^2, B^2, C^2, and D^2) and four interaction effects (AB, AC, BD, and CD).

3. Results and discussion

Based on the experimental design, model prediction and experimental removal (average of triplicate experimental results) are shown in Table 1.

Table 1
Experimental design and observed removal

Experimental design				Removal (%)					
				COD		NH_3–N		TOC	
A:H_2O_2/COD (molar ratio)	B:H_2O_2/Fe^{3+} (molar ratio)	C:$H_2O_2/C_2H_2O_4$ (molar ratio)	D:Time (min)	Predict	Exptl.	Predict	Exptl.	Predict	Exptl.
4.00	50.00	25.00	120.00	62.02	60.23	38.50	40.00	49.10	57.29
1.50	50.00	50.00	120.00	78.67	74.69	47.19	50.74	49.19	53.25
1.50	100.00	50.00	60.00	58.04	60.81	50.27	52.40	30.43	23.82
0.25	75.00	37.50	90.00	60.10	64.71	49.61	49.75	27.22	29.80
1.50	100.00	25.00	120.00	69.43	65.27	47.50	45.21	59.01	56.32
2.75	75.00	12.50	90.00	71.90	75.09	56.59	57.26	45.12	43.12
5.25	75.00	37.50	90.00	55.97	54.25	34.69	33.15	46.45	44.85
1.50	50.00	25.00	60.00	70.32	70.32	56.04	55.07	23.96	25.17
2.75	75.00	37.50	90.00	74.68	78.23	43.88	48.49	51.19	49.76
2.75	75.00	37.50	90.00	74.68	77.21	43.88	48.77	51.19	51.79
2.75	75.00	37.50	90.00	74.68	70.07	43.88	38.36	51.19	50.07
4.00	50.00	50.00	120.00	73.01	72.02	41.70	36.44	56.33	48.01
4.00	100.00	25.00	60.00	71.32	76.28	52.53	52.60	45.45	42.98
1.50	50.00	25.00	120.00	70.40	69.64	45.61	45.02	39.03	34.17
1.50	100.00	50.00	120.00	71.08	71.34	49.79	52.70	58.12	61.93
1.50	50.00	50.00	60.00	65.18	61.82	46.65	36.99	32.08	25.28
2.75	125.00	37.50	90.00	70.48	69.88	54.78	48.86	41.60	38.75
4.00	50.00	50.00	60.00	59.98	65.12	30.25	36.16	66.63	70.91
4.00	100.00	50.00	60.00	62.29	59.18	42.45	40.82	39.60	41.90
4.00	50.00	25.00	60.00	62.38	58.25	41.02	35.89	61.44	55.07
1.50	100.00	25.00	60.00	69.80	66.92	61.95	64.99	33.36	39.13
2.75	75.00	37.50	90.00	74.68	77.30	43.88	43.84	51.19	60.66
4.00	100.00	25.00	120.00	70.50	69.98	45.98	50.41	43.70	47.94
4.00	100.00	50.00	120.00	74.87	75.85	49.88	54.47	39.88	40.26
2.75	75.00	37.50	150.00	79.30	83.33	42.35	38.63	60.28	57.39
2.75	25.00	37.50	90.00	69.13	72.62	40.69	45.21	48.65	52.47
2.75	75.00	62.50	90.00	71.13	70.83	48.10	46.03	49.42	52.39
2.75	75.00	37.50	30.00	66.63	65.48	45.35	47.67	44.93	48.79
2.75	75.00	37.50	90.00	74.68	73.05	43.88	40.55	51.19	53.51
2.75	75.00	37.50	90.00	74.68	72.24	43.88	43.29	51.19	41.32

Table 2
ANOVA of the response parameters

Parameter	*F*-test	*p*-value	R^2	A.P.
COD	4.37	0.0037	0.8031	7.856
NH_3–N	3.35	0.0132	0.7579	8.803
TOC	4.87	0.0022	0.8196	8.992

3.1. Regression models and statistical analysis

To ascertain the suitability of the regression model and assess the interaction between the independent variables (operating conditions) and the dependent variables (responses) and subsequently obtain the "goodness of fit," analysis of variance (ANOVA) was performed. Fisher *F*-test value, *p*-value, coefficient of determination R^2, and adequate precision (A.P) are shown in Table 2. *F*-test value is a measure of variation of the data about the mean [27]. A *p*-value less than 0.05 indicates the suitability of the proposed models for treatment as there is no lack-of-fit. The models for COD, NH_3–N, and TOC removal (Y_1, Y_2, and Y_3) were significant by the *F*-test at 95% confidence level employed as all responses had a *p*-value < 0.05, and therefore, the removals fit the data well. The coefficient

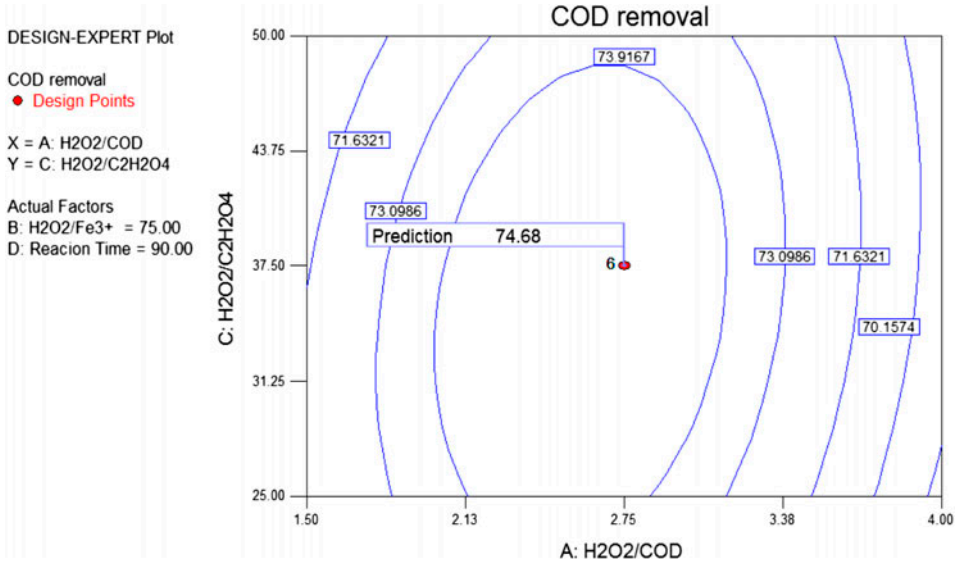

Fig. 2. Contour plot for COD removal.

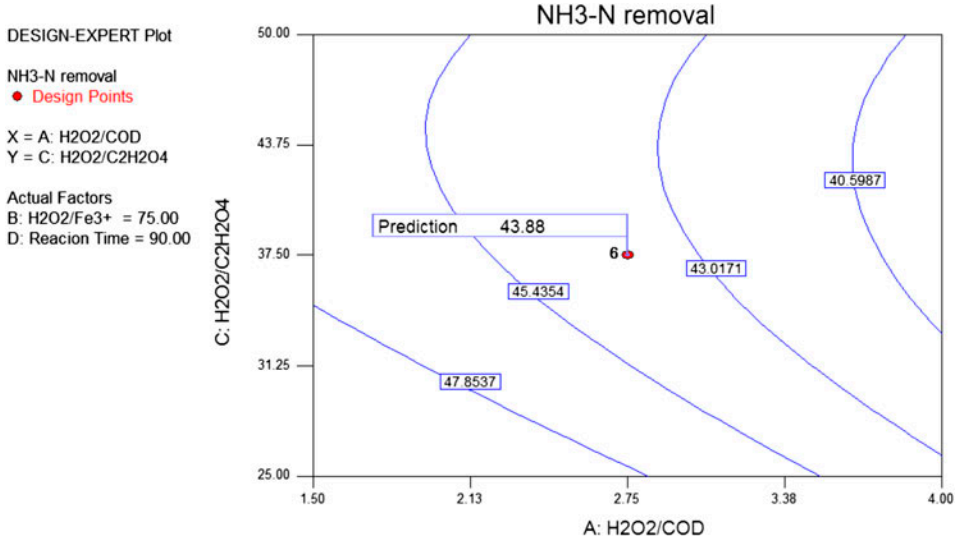

Fig. 3. Contour plot for NH_3–N removal.

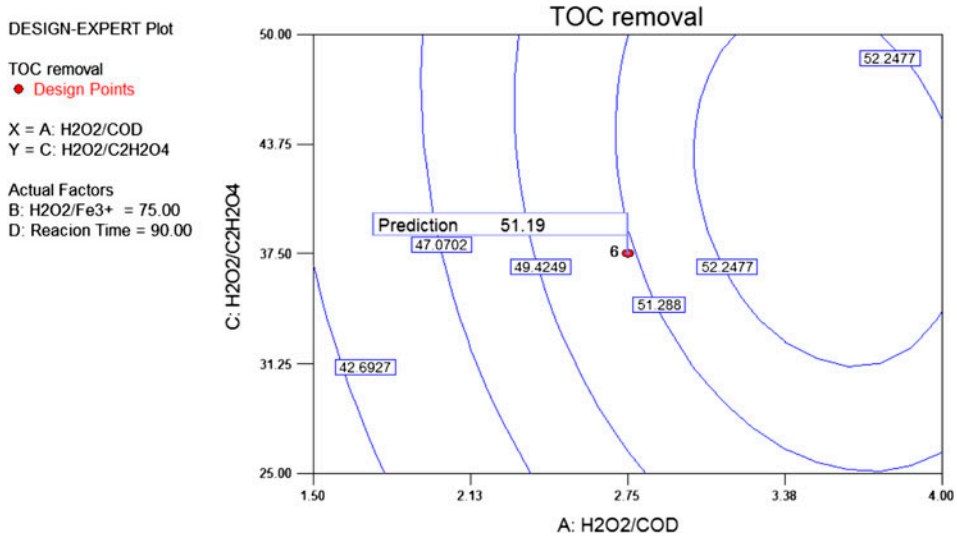

Fig. 4. Contour plot for TOC removal.

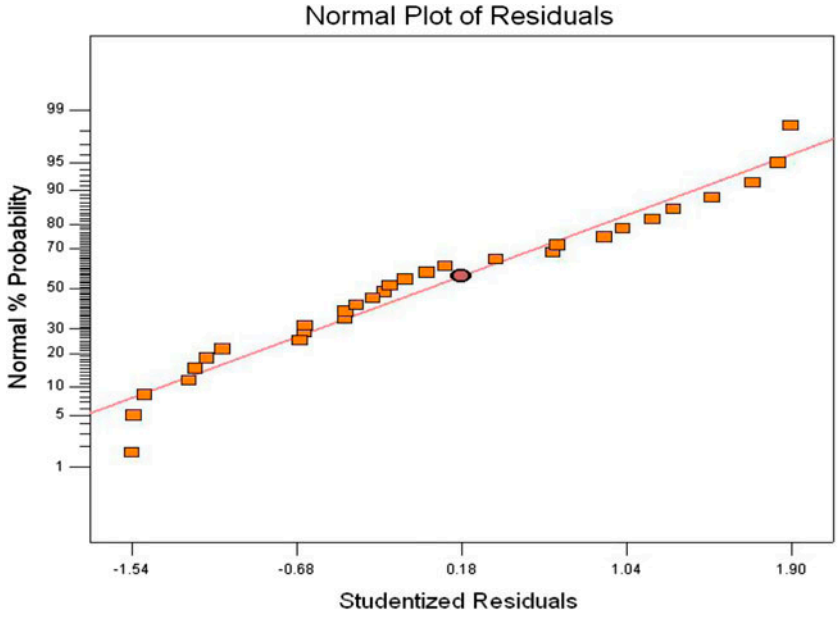

Fig. 5. Normal probability plot of the studentized residuals for COD removal.

of determination (R^2) is the proportion of variability in a data set which indicates whether the empirical model is good enough for the quadratic fit to navigate the design space defined by the CCD [28]. The R^2 value gives the proportion of the total variation in the response predicted by the model to the experimental data. The R^2 values were 0.8031 (COD), 0.7579 (NH_3–N), and 0.8196 (TOC). A.P. ratio compares the range of the predicted value at the design points to the average prediction error. Ratios greater than four indicate adequate model discrimination and can be used to navigate the design space defined by the CCD [28]. The A.P. for all the responses was greater than four. The ANOVA results indicate adequate agreement between the model prediction and experimental removal. The following fitted regression models were obtained to quantitatively investigate the effects of A: H_2O_2/COD molar ratio, B: H_2O_2/Fe^{3+} molar ratio, C: $H_2O_2/C_2H_2O_4$ molar ratio and D: reaction time on COD, TOC, and NH_3–N removal, respectively.

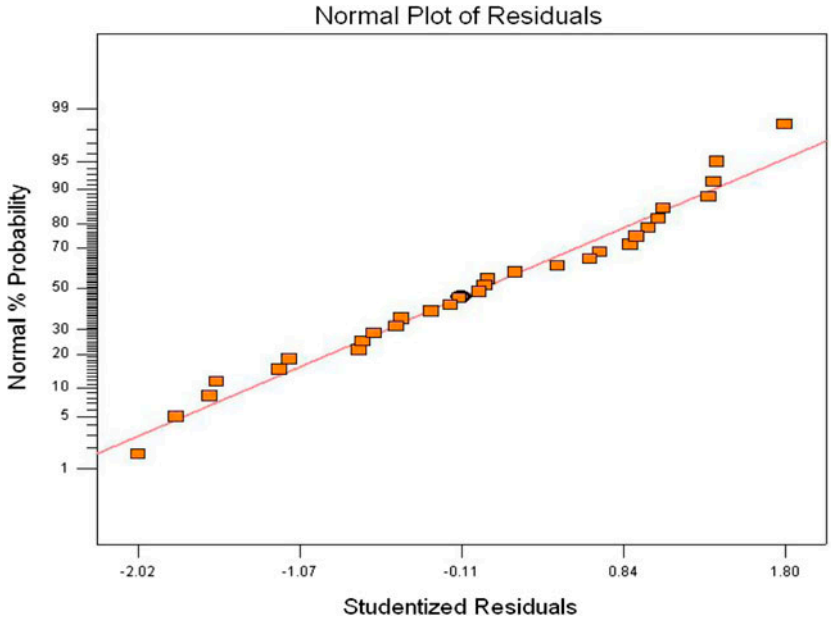

Fig. 6. Normal probability plot of the studentized residuals for NH_3–N removal.

COD removal

$$Y_1 = 74.68 - 1.03A + 0.34B - 0.19C + 3.17D - 4.16A^2 - 1.22B^2 - 0.79C^2 + -0.43D^2 + 2.36AB + 0.68AC - 0.11BD + 3.35CD \quad (8)$$

NH_3–N removal

$$Y_2 = 43.88 - 3.73A + 3.52B - 2.12C - 0.75D - 0.43A^2 + 0.96B^2 + 2.12C^2 - 8.437E - 003D^2 + 1.40AB + 0.40AC + 1.98AD + 0.18BC - 1.01BD + 3.49CD \quad (9)$$

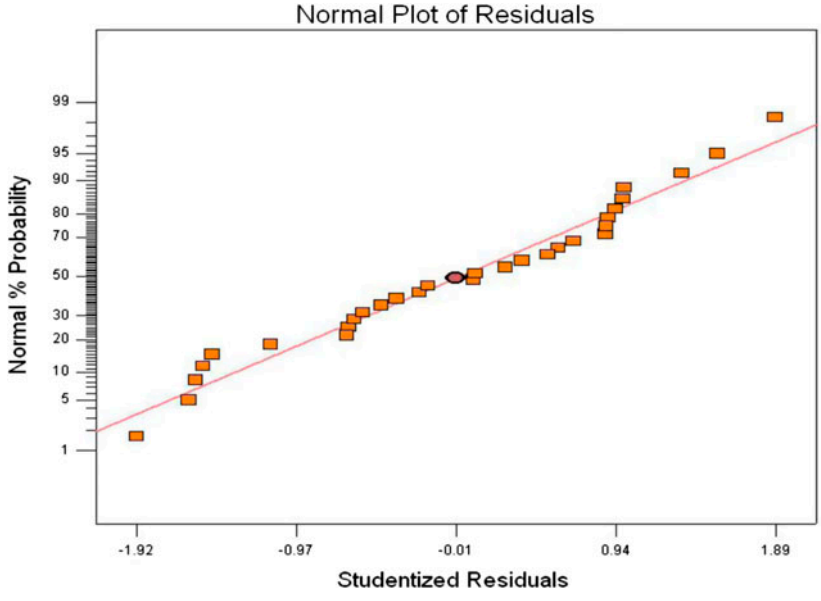

Fig. 7. Normal probability plot of the studentized residuals for TOC removal.

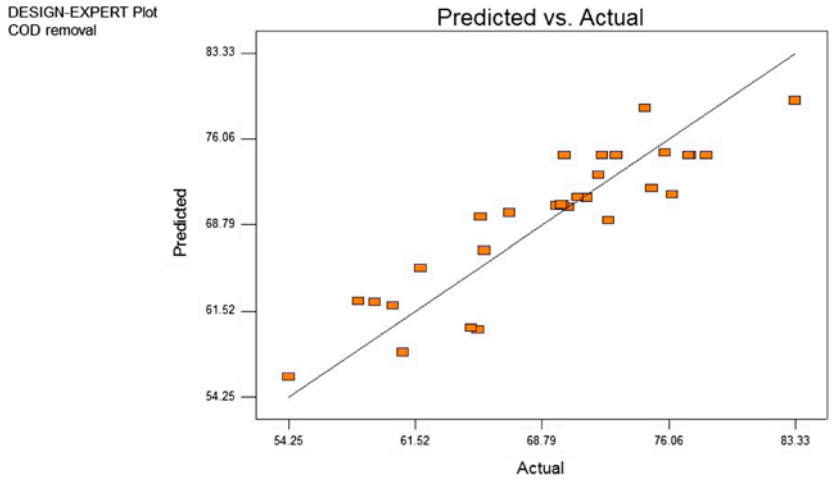

Fig. 8. Plot of the predicted vs. actual COD removal.

TOC removal

$$Y_3 = 51.19 + 4.81A - 1.76B + 1.08C + 3.84D - 3.59A^2 - 1.52B^2 - 0.98C^2 + 0.35D^2 - 6.35AB - 0.73AC - 6.85AD - 2.76BC + 2.65BD + 0.51CD \quad (10)$$

In Eqs. (8)–(10), the values of the sum of a constant (β_o), (74.68, 43.88, and 51.19) represent the percentage removal of COD, NH_3–N, and TOC, respectively. The positive sign indicates that the variable is directly proportional to the response (COD, NH_3–N, and TOC removal) and the negative sign indicates that the variable is inversely proportional to the response.

3.2. Process analysis

Visualization of the predicted model equation can be obtained from the contour plot [26]. A contour plot is a two dimensional display of the surface plot and in the contour plot, lines of constant response are drawn in the plane of the variables. The contour plot helps to visualize the shape of a response surface. When the contour plot displays ellipses or circles, the center of the system refers to a point of maximum or minimum response. Sometimes, contour plot may display hyperbolic or parabolic system of the contours [29]. Figs. 2–4 shows the contour plots for COD, NH_3–N, and TOC removal. Decreasing oxalate (increasing $H_2O_2/C_2H_2O_4$ molar ratio), and increasing H_2O_2 (increasing H_2O_2/COD molar ratio) will reduce COD removal, increasing oxalate (decreasing $H_2O_2/C_2H_2O_4^+$ molar ratio) and increasing H_2O_2 (increasing H_2O_2/COD molar ratio) will reduce NH_3–N removal and increasing oxalate (decreasing $H_2O_2/C_2H_2O_4$ molar ratio) and decreasing H_2O_2 (decreasing H_2O_2/COD molar ratio) simultaneously

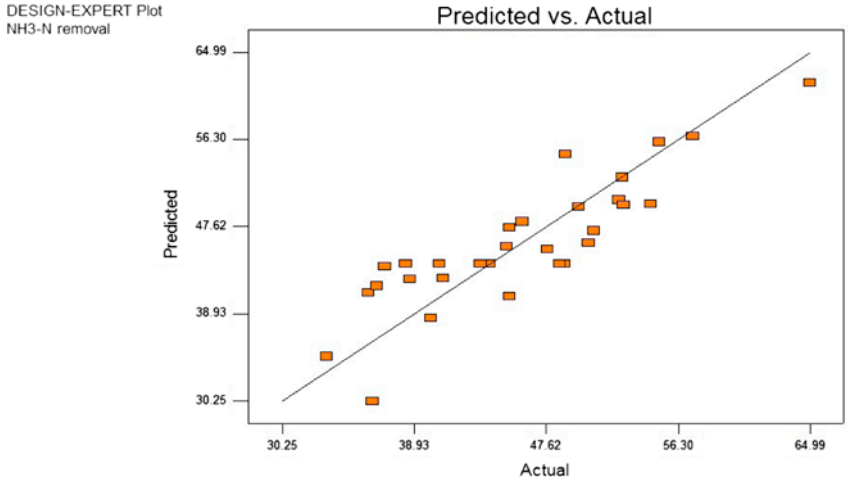

Fig. 9. Plot of predicted vs. actual for NH_3–N removal.

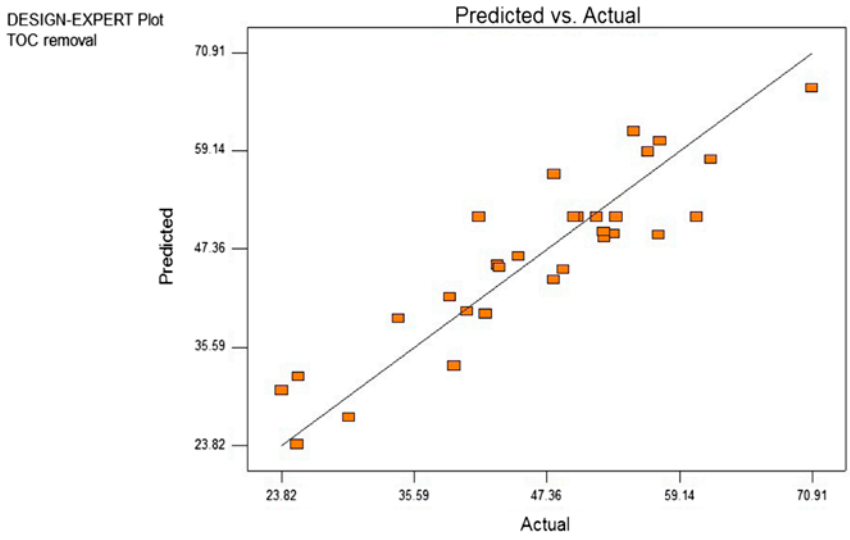

Fig. 10. Plot of predicted vs. actual for TOC removal.

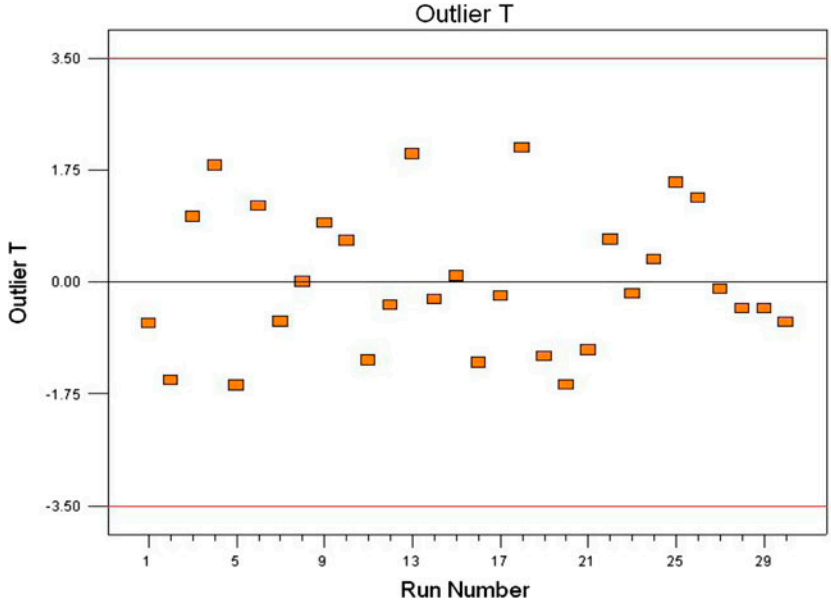

Fig. 11. Outlier T plot for COD removal.

or one at a time will reduce TOC removal at H_2O_2/Fe^{3+} molar ratio 75.0 and reaction time 90 min in all three cases. The adequacy of the models was also evaluated by the residuals i.e. difference between the observed and the predicted response value. Normal probability plot of the studentized residuals (Figs. 5–7) and plot of predicted vs. actual removal (Figs. 8–10) indicate that there is no abnormalities in the model as all data were found around the line of "best fit". In the outlier T plots (Figs. 11–13), all three responses (COD, NH_3–N, and TOC removal) were within the top (+3.5) and bottom (-3.5) detection limits, indicating applicability of the model. Figures 14–16 shows the perturbation plots for COD, NH_3–N, and TOC removal. The plots show how response (COD, NH_3–N and TOC removal) changes as each variable (A: H_2O_2/COD molar ratio, B: H_2O_2/Fe^{3+} molar ratio, C: $H_2O_2/C_2H_2O_4$ molar ratio, and D: reaction time) moves from the chosen reference point, that is, 0 (central) level, with other variables held constant at the reference value.

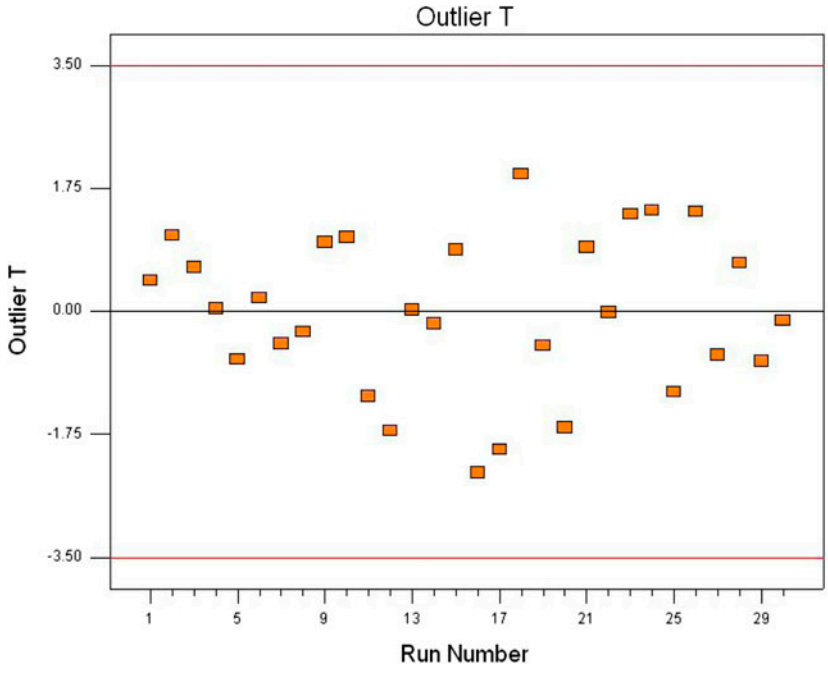

Fig. 12. Outlier T plot for NH_3–N removal.

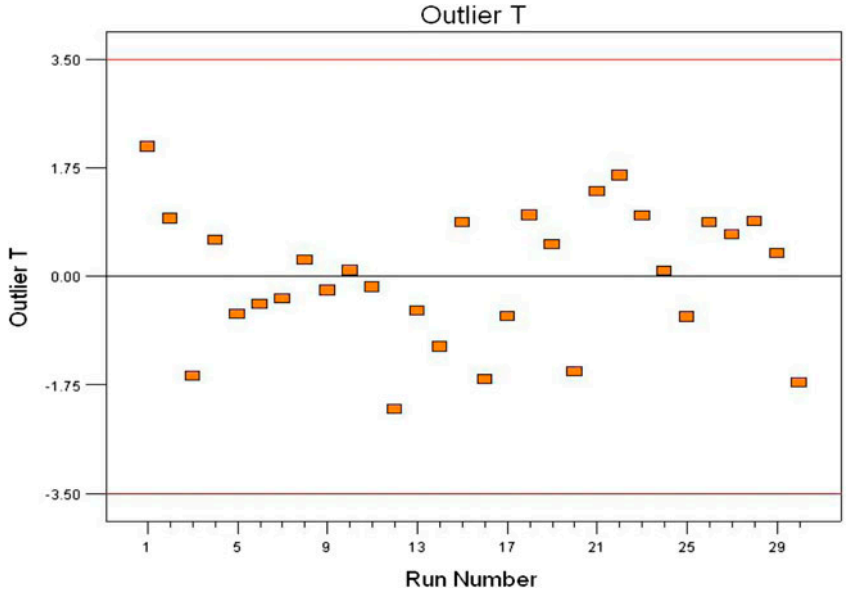

Fig. 13. Outlier T plot for TOC removal.

3.3. Optimization and model verification

Numerical optimization was used to determine the optimum operating conditions for COD, NH_3–N, and TOC removal. Based on the response surface and desirability functions (figure not shown), the optimum operating conditions were obtained. In this case, all responses were targeted to be in range and were goaled to be maximized. The optimum conditions were obtained for highest desirability at H_2O_2/COD molar ratio 2.75, H_2O_2/Fe^{3+} molar ratio 75, $H_2O_2/C_2H_2O_4$ molar ratio 37.5 and reaction time 90 min at pH 3. Under these operating conditions, 74.68, 43.88, and 51.19% removal of COD, NH_3–N, and TOC,

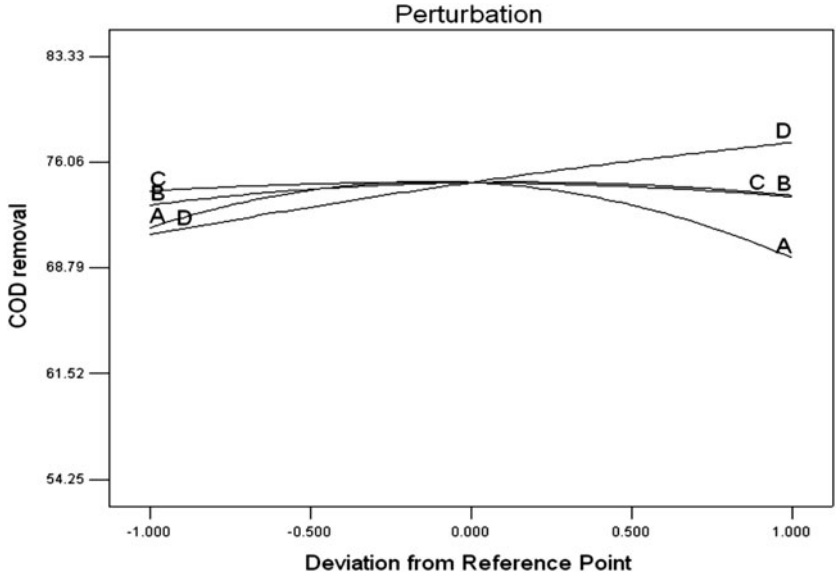

Fig. 14. Perturbation plot for COD removal.

respectively was predicted based on desirability function of 1.00. Three confirmatory experiments were conducted under the optimum operating conditions to verify the model prediction. Model prediction and experimental removal efficiency were in agreement with < 5% error (Table 3).

3.4. Effect of pH

The pH is an important parameter of the UV-vis/ferrioxalate/H_2O_2 process. At pH 2–3, the predominant ferrioxalate complex $Fe^{III}(C_2O_4)_3^{3-}$ is highly photosensitive and reduction of Fe^{3+} to Fe^{2+}, through a photoinduced ligand to metal charge transfer, can occur over the ultraviolet and into the visible [7]. At higher pH 4–5, the ferrioxalate complexes are less photosensitive. In addition, above pH 4–5, process efficiency decreases since coagulation of the ferrioxalate complexes reduces the catalytic effect of Fe^{2+} to decompose H_2O_2 [30]. To study the effect of pH on process efficiency (COD, NH_3–N, and TOC removal), experiments were conducted under the optimum

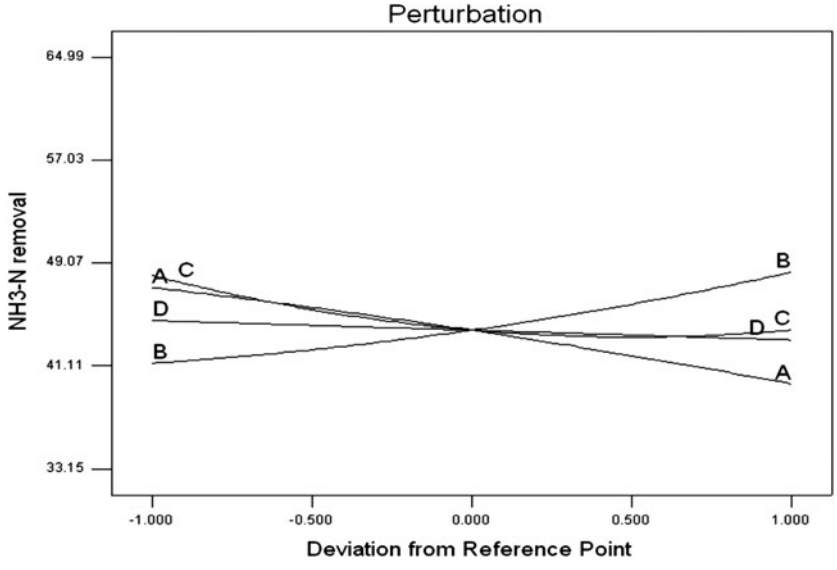

Fig. 15. Perturbation plot for NH_3–N removal.

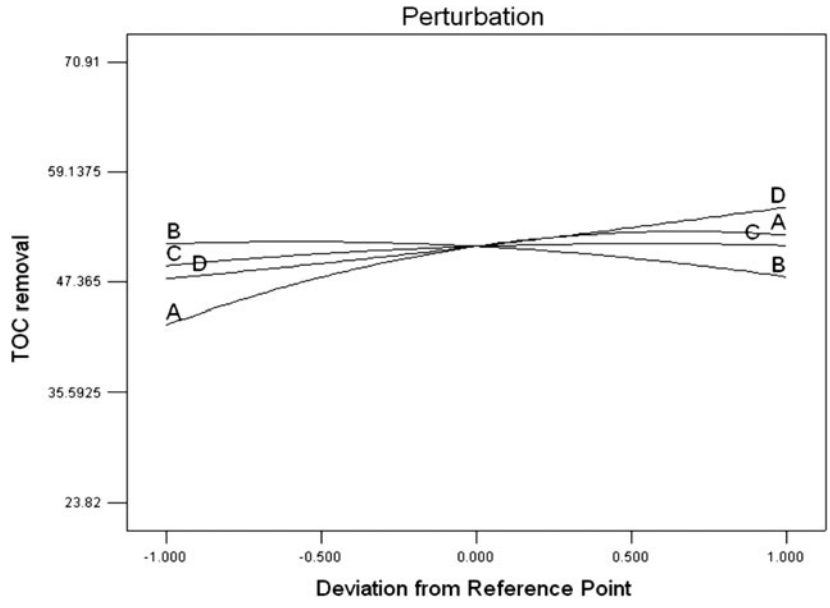

Fig. 16. Perturbation plot for TOC removal.

Table 3
Model prediction and experimental removal efficiency

Parameter	Model prediction	Experimental removal (%)	Error	% Error
COD removal (%)	74.68	78.32,77.55,79.25; Av.78.37	3.69	4.71
NH_3–N removal (%)	43.88	46.58,46.3,44.93 ; Av. 45.94	2.06	4.48
TOC removal (%)	51.19	52.94,51.93,52.02; Av. 52.30	1.11	2.12

operating conditions (H_2O_2/COD molar ratio 2.75, H_2O_2/Fe^{3+} molar ratio 75, $H_2O_2/C_2H_2O_4$ molar ratio 37.5 and reaction time 90 min). At pH 2, 3, 4, and 5 COD removal were 72.36, 78.37, 75.26, and 71.10%; NH_3–N removal were 44.38, 45.94, 44.66, and 44.11%; and TOC removal were 51.64, 52.3, 49.49, and 50.93%, respectively. Maximum process efficiency was achieved at pH 3 as seen in Fig. 17.

3.5. Biodegradability

Under optimum operating conditions (H_2O_2/COD molar ratio 2.75, H_2O_2/Fe^{3+} molar ratio 75, $H_2O_2/C_2H_2O_4$ molar ratio 37.5, reaction time 90 min and pH 3), UV-vis/ferrioxalate/H_2O_2 treatment of the antibiotic aqueous solution improved the biodegradability (BOD_5/COD ratio) from 0 to 0.35, indicating that the

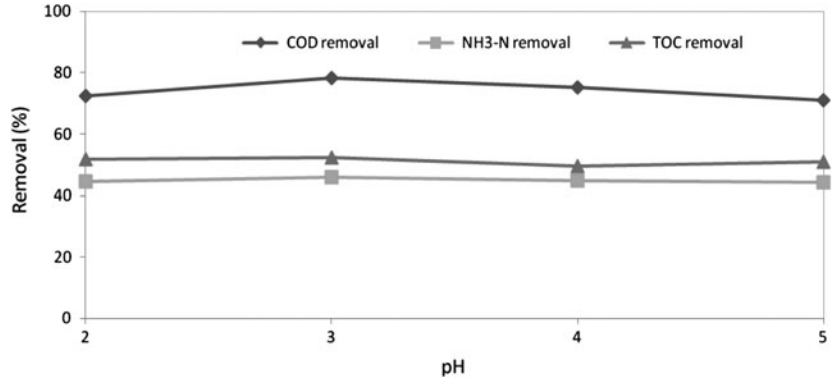

Fig. 17. Effect of pH.

treated antibiotic aqueous solution was amenable to biological treatment [31]. Similar biodegradability improvement (0 to 0.37 and 0.40) was observed in Fenton and photo-Fenton treatment of aqueous solution of antibiotics amoxicillin, ampicillin, and cloxacillin [23,24]. Even though COD and TOC removal (78.37 and 52.30%) was not very high, the treatment produced and effluent of BOD_5/COD ratio 0.35 in 90 min, which is amenable to subsequent biological treatment. Trovo et al. [32] observed 73% TOC removal in much longer reaction time of 240 min.

4. Conclusions

The optimum operating conditions for modified photo-Fenton (UV-vis/Ferrioxalate/H_2O_2) treatment of a 300 mg/L antibiotic aqueous solution (150 mg/L of amoxicillin and 150 mg/L of cloxacillin) obtained by using the CCD of the RSM were H_2O_2/COD molar ratio 2.75, H_2O_2/Fe^{3+} molar ratio 75, $H_2O_2/C_2H_2O_4$ molar ratio 37.5, reaction time 90 min and pH 3. Under optimum operating conditions, 78.37, 45.94, and 52.30% removal of COD, NH_3–N, and TOC, respectively, were achieved and the biodegradability (BOD_5/COD ratio) improved from 0 to 0.35. Model prediction and experimental removal efficiency were in agreement with < 5% error. The modified photo-Fenton process is effective in pretreatment of the antibiotic aqueous solution for biological treatment.

Acknowledgment

The authors are thankful to the management and authorities of the Universiti Teknologi PETRONAS for providing facilities for this research.

References

[1] M. Pera-Titus, V. Garcia-Molina, M.A. Banos, J. Gimenez, S. Esplugas, Degradation of chlorophenols by means of advanced oxidation processes: A general review, Appl. Catal. B 4 (2004) 219–256.
[2] J. Kiwi, C. Pulgarin, P. Peringer, Effect of Fenton and photo-Fenton reaction on the degradation and biodegradability of 2- and 4-nitrophenols in water treatment, Appl. Catal. B 4 (1994) 335–350.
[3] J.P. Scott, D.F. Ollis, Integration of chemical and biological oxidation processes for water treatment: Review and recommendations, Environ. Prog. 14 (1995) 88–103.
[4] C. Walling, Fenton's reagent revisited, Acc. Chem. Res. 8 (1975) 125–131.
[5] J.J. Pignatello, D. Liu, P. Houston, Evidence for an additional oxidant in the photo assisted Fenton reaction, Environ. Sci. Technol. 33 (1999) 1832–1839.
[6] A. Safarzadeh-Amiri, J.R. Bolton, S.R. Cater, Ferrioxalate-mediated photodegradation of organic pollutants in contaminated water, Water Res. 31 (1997) 787–798.
[7] K.A. Hislop, J.R. Bolton, The photochemical generation of hydroxyl radicals in the UV-vis/ferrioxalate/ H_2O_2 system, Environ. Sci. Technol. 33 (1999) 3119–3126.
[8] N. Zhang, J. Huang, W. Zheng, Research on photo degradation of aniline wastewater by dynamic UV-vis/H_2O_2/ferrioxalate complexes process, J. Chem. Ind. Eng. 53 (2002) 36–39.
[9] P. Tripathi, M. Chaudhuri, Decolourisation of metal complex azo dyes and treatment of a dyehouse waste by modified photo-Fenton (UV-vis/ferrioxalate/H_2O_2) process, Indian J. Eng. Mat. Sci. 11 (2004) 499–504.
[10] J.M. Monteagudo, A. Durán, J.M. Corral, A. Carnicer, J.M. Frades, M.A. Alonso, Ferrioxalate-induced solar photo-Fenton system for treatment of winery wastewater, Chem. Eng. J. 181–182 (2012) 281–288.
[11] Y. Lee, J. Jeong, C. Lee, S. Kim, J. Yoon, Influence of various reaction parameters on 2,4-D removal in photo/ferrioxalate/H_2O_2 process, Chemosphere 51 (2003) 901–912.
[12] D. Zhou, F. Wu, N. Deng, Fe (III)-oxalate complexes induced photooxidation of diethylstilbestrol in water, Chemosphere 57 (2004) 283–291.
[13] M.S. Lucas, J.A. Peres, Degradation of Reactive Black 5 by Fenton/UV-C and ferrioxalate/H_2O_2/solar light processes, Dyes Pigm. 74 (2007) 622–629.
[14] M. Chaudhuri, T.Y. Wei, Decolourisation of reactive dyes by modified photo-fenton process under irradiation with sunlight, Nat. Env. Poll. Technol. 8 (2009) 359–363.
[15] J.M. Monteagudo, A. Durán, J.M. Corral, A. Carnicer, J.M. Frades, M.A. Alonso, Catalytic degradation of Orange II in a ferrioxalate-assisted photo-Fenton process using combined UV-A/C-solar pilot-plant system, Appl. Catal. B 95 (2010) 120–129.
[16] J.M. Monteagudo, A. Durán, M. Aguirre, I. San Martín, Optimization of the mineralization of a mixture of phenolic pollutants under a ferrioxalate-induced solar photo-Fenton process, J. Hazard. Mater. 185 (2011) 131–139.
[17] M.V. Walter, J.W. Vennes, Occurrence of multiple-antibiotic resistant enteric bacteria in domestic sewage and oxidative lagoons, Appl. Environ. Microbiol. 50 (1985) 930–933.
[18] Standard Methods for the Examination of Water and Wastewater, 21st edition, American Public Health association, American Water Works Association and Water Environment Federation, Washington, 2005.
[19] I. Talinli, G.K. Anderson, Interference of hydrogen peroxide on the standard COD test, Water Res. 26 (1992) 107–110.
[20] Y.W. Kang, M.J. Cho, K.Y. Hwang, Correction of hydrogen peroxide interference on standard chemical oxygen demand test, Water Res. 33 (1999) 1247–1251.
[21] Water Analysis Handbook, fourth ed., Hach Company, Loveland, CO., 2002.
[22] I. Arslan-Alaton, S. Dogruel, Pre-treatment of penicillin formulation effluent by advanced oxidation processes, J. Hazard. Mater. B112 (2004) 105–113.
[23] E. Elmolla, M. Chaudhuri, Optimization of Fenton process for treatment of amoxicillin, ampicillin and cloxacillin antibiotics in aqueous solution, J. Hazard. Mater. 170 (2009) 666–672.
[24] E. Elmolla, M. Chaudhuri, Degradation of amoxicillin, ampicillin and cloxacillin antibiotics in aqueous solution by the photo Fenton process, J. Hazard. Mater. 172 (2009) 1476–1481.
[25] Design-Expert® Software, Version 6.0.7, User's guide (2002).
[26] M.A. Bezerra, R.E. Santelli, E.P. Oliveira, L.S. Villar and L. and A. Escaleira, Review: Response surface methodology (RSM) as a tool for optimization in analytical chemistry, Talanta 76 (2008) 965–977.
[27] M.Y. Noordin, V.C. Venkatesh, S. Sharif, S. Elting, A. Abdullah, Application of response surface methodology in describing the performance of coated carbide tools when turning AISI 1045 steel, J. Mater. Proc. Technol. 145 (2004) 46–58.
[28] S. Ghafari, H.A. Aziz, M.H. Isa, A.A. Zinatizadeh, Application of response surface methodology (RSM) to optimize coagulation flocculation treatment of leachate using poly-aluminium chloride (PAC) and alum, J. Hazard. Mater. 163 (2009) 650–656.

[29] R.H. Myers, D.C. Montgomery, Response surface methodology: Process and product optimization using designed experiments, John Wiley & Sons, Inc., New York, NY, 1995.
[30] J.M. Monteagudo, A. Duran, M. Aguirre, I. San Martin, Photodegradation of Reactive Blue 4 solutions under ferrioxalate-assisted UV/solar photo-Fenton system with continuous addition of H_2O_2 and air injection, Chem. Eng. J. 162 (2010) 702–709.
[31] F. Al-Momani, E. Touraud, J.R. Degorce-Dumas, J. Roussy, O. Thomas, Biodegradability enhancement of textile dyes and textile wastewater by VUV photolysis, J. Photochem. Photobiol. A. 153 (2002) 191–197.
[32] A.G. Trovó, R.F. Pupo Nogueira, A. Agüera, A.R. Fernandez-Alba, S. Malato, Degradation of the antibiotic amoxicillin by photo-Fenton process—Chemical and toxicological assessment, 45 (2011) 1394–1402.